A Fully Analytical Model for the Series Impedance of Through-Silicon Vias With Consideration of Substrate Effects and Coupling With Horizontal Interconnects

Chuan Xu, *Student Member, IEEE*, Vassilis Kourkoulos, *Member, IEEE*, Roberto Suaya, *Senior Member, IEEE*, and Kaustav Banerjee, *Senior Member, IEEE*

***Abstract*—This paper introduces a fully analytical and physical model capable of extracting high-frequency series impedance of through-silicon vias (TSVs) in 3-D integrated chips with consideration of the eddy currents in the surrounding Si substrate and coupling with horizontal interconnects. The model employs the vertical-to-vertical and horizontal-to-vertical 3D vector potential Green's function in layered media and is concise and sufficiently accurate in the entire range of interest for both the frequency and the center-to-center distance between TSVs. Along with the series impedances between horizontal wires, which are extracted from the discrete complex image method, as well as the TSV and horizontal wire capacitance values, the total loop impedance can be obtained. Our approach is verified against a full-wave finite-element-method electromagnetic solver High Frequency Structure Simulator, and it shows good accuracy ($< 7\%$ error) in the entire frequency range examined (up to 100 GHz). Given the fact that the formulated TSV series impedance model is purely analytical, the model could be efficiently used for system-level interconnect impedance extraction in emerging 3-D integrated systems.**

***Index Terms*—Analytical impedance modeling, eddy currents, Green's function, high frequency, interconnect, quasi-magnetostatic, substrate effects, through-silicon via (TSV), 3-D integrated circuits.**

I. Introduction

THREE-DIMENSIONAL integrated chips (3-D ICs), where multiple active layers or substrates are vertically stacked on top of each other and interconnected using "short" vertical links, have been shown to reduce on-chip global interconnect lengths and thereby alleviate delay and power consumption problems [1]. Three-dimensional ICs also facilitate the integration of dissimilar technologies (digital, analog, radio-frequency circuits, etc) or materials (Si, III–V, or graphene) on different active layers [1], [2]. As shown in Fig. 1, the interconnects in 3-D ICs include horizontal wires, short vias, and through-silicon vias (TSVs). The TSVs that are high-aspect-ratio vertical interconnects, providing connectivity between active layers, constitute a key component for 3-D ICs.

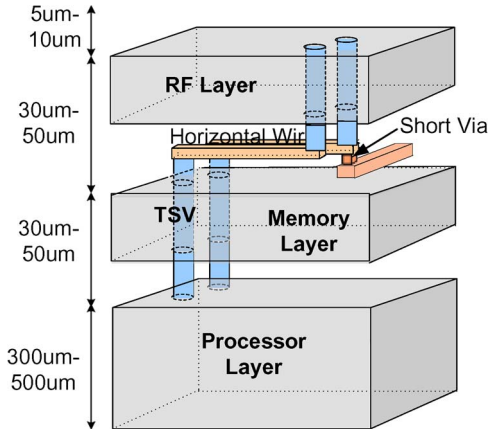

Fig. 1. Schematic view of a 3-D IC.

While fabrication technologies for TSVs have progressed [3]–[6], accurate and efficient TSV impedance evaluation is required for performance evaluation of circuits and systems built in 3-D ICs and for design optimization of 3-D IC interconnects, including TSVs. Unfortunately, all published approaches are either inaccurate, or inefficient, or present poor scalability. For example, impedance models provided in [7] and [8] do not even consider the substrate eddy-current effect. Some empirical models for TSV impedance are provided in [9], and the authors claim to have taken into account the substrate loss. However, there is no parameter representing the silicon conductivity in their model, which implies that their empirical formulas lack generality. Full-wave finite-element-method (FEM) simulations [10] are accurate but very slow and memory intensive, and as such, they are not suitable for large-scale analysis and design optimization. Physical impedance/admittance transmission line models for the TSVs are developed in [11] and [12] with consideration of the substrate alternating-current conduction and eddy currents. However, the models assume a 2D configuration, or in other words, the models, particularly the

Manuscript received March 24, 2011; revised June 4, 2011; accepted July 1, 2011. Date of current version September 21, 2011. This work was supported in part by the National Science Foundation under Grant CCF-0917385 and in part by University of California Discovery under Grant COM09S-156729. The review of this paper was arranged by Editor M. Ieong.

C. Xu and K. Banerjee are with the Department of Electrical and Computer Engineering, University of California Santa Barbara, Santa Barbara, CA 93106 USA (e-mail: chuanxu@ece.ucsb.edu; kaustav@ece.ucsb.edu).

V. Kourkoulos and R. Suaya are with the Calibre Division, Mentor Graphics Corporation, 38334 Saint Ismier, France (e-mail: vassilis_kourkoulos@mentor.com; roberto_suaya@mentor.com).

Color versions of one or more of the figures in this paper are available online at http://ieeexplore.ieee.org.

Digital Object Identifier 10.1109/TED.2011.2162846

series impedance models, are only accurate when the TSV height is much larger than the center-to-center (c2c) distance between TSVs. Finally, similar to the approach taken by researchers for horizontal interconnects [13]–[18], one can also employ numerical methodologies in computational electromagnetics to analyze TSVs [19]. However, this is still far from achieving the same efficiency as analytical models.

In this paper, a 3D physical model of TSV series impedance with the inclusion of substrate eddy-current effects and horizontal interconnects to TSV coupling is obtained step by step. The model is proved to cause tolerable errors in any practical situation, whereas its tremendous advantage is obvious, i.e., concise equations for TSV series impedance can be obtained. The loop impedance is obtained and verified against a full-wave FEM software (High Frequency Structure Simulator (HFSS) [20]) by embedding the model into the loop impedance extraction of an interconnect loop containing both TSVs and horizontal wires.

II. Three-Dimensional Vector Potential Green's Function

Up to 100 GHz, the electromagnetic (EM) quarter wavelength in SiO_2 is greater than 0.37 mm, which is much greater than the TSV dimension ($\sim$30 μm). Therefore, quasi-magnetostatic and quasi-electrostatic approaches can be employed. In 3D quasi-magnetostatic approximation, the vector potential in layered media at any (x, y, z) due to a monopole current source at (x', y', z') can be expressed as

$$\overrightarrow{A}(x,y,z) = \mu_0 \left\langle \underline{\underline{G}}^A(x,y,z;x',y',z'); \overrightarrow{J}(x',y',z') \right\rangle \quad (1)$$

where μ_0 is the vacuum permeability (the permeability values in silicon, copper, and SiO_2 are almost the same as in vacuum); "$\langle ; \rangle$" is the space integration operator, which captures the entire space integration of sources at various (x', y', z'); $\vec{J}(x', y', z')$ is the current density at (x', y', z'); $\underline{\underline{G}}^A(x, y, z; x', y', z')$ is called the space-domain vector potential Green's function, which is a second-order tensor [21], i.e.,

$$\underline{\underline{G}}^A = \begin{bmatrix} G^A_{\rm xx} & 0 & 0 \\ 0 & G^A_{\rm yy} & 0 \\ G^A_{\rm zx} & G^A_{\rm zy} & G^A_{\rm zz} \end{bmatrix}. \quad (2)$$

The components in $\underline{\underline{G}}^A$ can be transformed from the spectral-domain vector potential Green's function $\underline{\underline{\tilde{G}}}^A$

$$G^A_{\rm xx}(\Delta\rho, z, z') = G^A_{\rm yy}(\Delta\rho, z, z') = \frac{1}{2\pi}\int_0^\infty \tilde{G}^A_{\rm uu}(\lambda, z, z'){\rm J}_0(\lambda\cdot\Delta\rho)\lambda\, d\,\lambda \quad (3a)$$

$$G^A_{\rm zz}(\Delta\rho, z, z') = \frac{1}{2\pi}\int_0^\infty \tilde{G}^A_{\rm zz}(\lambda, z, z'){\rm J}_0(\lambda\cdot\Delta\rho)\lambda\, d\,\lambda \quad (3b)$$

$$G^A_{\rm zx}(\Delta\rho, \phi, z, z') = -\frac{j\cos(\phi)}{2\pi}\int_0^\infty \tilde{G}^A_{\rm zu}(\lambda, z, z'){\rm J}_1(\lambda\cdot\Delta\rho)\lambda\, d\,\lambda \quad (3c)$$

$$G^A_{\rm zy}(\Delta\rho, \phi, z, z') = -\frac{j\sin(\phi)}{2\pi}\int_0^\infty \tilde{G}^A_{\rm zu}(\lambda, z, z'){\rm J}_1(\lambda\cdot\Delta\rho)\lambda\, d\,\lambda \quad (3d)$$

where $\Delta\rho = \sqrt{(x'-x)^2 + (y'-y)^2}$ is the horizontal distance between the source and observation points; ϕ is the angle of the line from the source to the observation point with respect to the x-axis, or in other words, $\cos(\phi) = (x'-x)/\Delta\rho$ and $\sin(\phi) = (y'-y)/\Delta\rho$; λ is the horizontal component of wave vector $\vec{k}$ ($\lambda = \sqrt{k_x^2 + k_y^2}$);[1] $\tilde{G}^A_{\rm uu}$, $\tilde{G}^A_{\rm zz}$, and $\tilde{G}^A_{\rm zu}$ are the components in $\underline{\underline{\tilde{G}}}^A$ representing horizontal-to-horizontal (h2h) interaction, vertical-to-vertical (v2v) interaction, and horizontal-to-vertical (h2v) interaction, respectively; and $\rm J_0$ and $\rm J_1$ are the zeroth- and first-order Bessel functions of the first type, respectively. The expressions for $\tilde{G}^A_{\rm uu}$, $\tilde{G}^A_{\rm zz}$, and $\tilde{G}^A_{\rm zu}$ can be obtained from the transmission line Green's functions of a layered media [21].

The Green's function tensor in (2) is not symmetric with respect to the source and observation points, resulting in vertical-to-horizontal (v2h) interaction (which is 0) not being equal to h2v interaction, which violates reciprocity requirements. To account for reciprocity, one recipe [21] includes a correction factor C^Φ to the second-order Green tensor, making it symmetric with respect to the source and observation points and satisfying the boundary conditions [13], [22],[2] i.e.,

$$\underline{\underline{G}}^{A\,{\rm and}\,C^\Phi} = \begin{bmatrix} G^A_{\rm xx} & 0 & G^{C^\Phi}_{\rm xz} \\ 0 & G^A_{\rm yy} & G^{C^\Phi}_{\rm yz} \\ G^A_{\rm zx} & G^A_{\rm zy} & G^A_{\rm zz} + G^{C^\Phi}_{\rm zz} \end{bmatrix} \quad (4)$$

where $G^{C^\Phi}_{\rm xz}(x, y, z; x', y', z') = G^A_{\rm zx}(x', y', z'; x, y, z)$, $G^{C^\Phi}_{\rm yz}(x, y, z; x', y', z') = G^A_{\rm zy}(x', y', z'; x, y, z)$, and $G^A_{\rm zz}(x, y, z; x', y', z') + G^{C^\Phi}_{\rm zz}(x, y, z; x', y', z') = G^A_{\rm zz}(x', y', z'; x, y, z) + G^{C^\Phi}_{\rm zz}(x', y', z'; x, y, z)$.

In a typical interconnect structure in 3-D ICs (e.g., a TSV-horizontal wire loop shown in Fig. 2), both the TSVs and horizontal wires are required. However, the complexities involved in extracting the self and mutual series impedance of h2h, v2v, and h2v are quite different.

[1] Some terminology definitions used in this paper are different from those in [21] but are consistent with [14] and/or [16]: λ in this paper is the same as k_ρ in [21]; σ_i in this paper is the same as $j\omega\varepsilon_{\rm ri}\varepsilon_0$ in [21]; and γ_i in this paper is the same as jk_i in [21].

[2] The two sets of vector potential Green's function are not contradictory. $\underline{\underline{G}}^A$ is essentially a magnetic dyadic Green's function (according to [21, eq. (38)], whereas $\underline{\underline{G}}^{A\,{\rm and}\,C^\Phi}$ is a mixed potential dyadic Green's function, in which the terms related to C^Φ arise from part of the electrical scalar potential when both horizontal and vertical current components are present [21], [22]. $\underline{\underline{G}}^A$ and $\underline{\underline{G}}^{A\,{\rm and}\,C^\Phi}$ are equivalent in the sense that the double loop integration of the source and observation points (or mutual loop impedance divided by $j\omega\mu_0$) is the same.

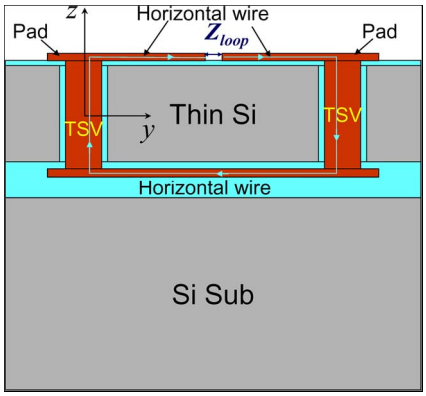

Fig. 2. Cross-sectional view of a TSV horizontal wire loop.

A. Extraction of the h2h Component of Vector Potential Green's Functions

The space-domain $G^A_{\rm xx}$ and $G^A_{\rm yy}$ can be analytically obtained from the well-known discrete complex image method (DCIM) approximation of $\tilde{G}^A_{\rm uu}$, when the source and observation points are in the same layer or in a different layer but with the same complex effective conductivity $\sigma_i = \sigma_{i,\rm DC} + j\omega\varepsilon_i$ [ω is the radial frequency; $\sigma_{i,\rm DC}$ and ε_i are the direct-current (DC) conductivity and the dielectric permittivity of the layer where the observation point lies].[1] In DCIM, $\tilde{G}^A_{\rm uu}$ can be approximated as the sum of several exponentials divided by $\sqrt{\lambda^2+\gamma_i^2}$ [13]–[18], where $\gamma_i = \sqrt{j\omega\mu_0\sigma_i}^{-1}$. The space-domain Green's function can then be analytically obtained from the integration

$$\int_0^\infty \frac{e^{-\sqrt{\lambda^2+\gamma_i^2}\cdot f(z,z')}}{\sqrt{\lambda^2+\gamma_i^2}} \cdot \mathrm{J}_0(\lambda\cdot\Delta\rho)\lambda\, d\,\lambda = \frac{e^{-\gamma_i\sqrt{\Delta\rho^2+f(z,z')^2}}}{\sqrt{\Delta\rho^2+f(z,z')^2}} \tag{5}$$

where $f(z,z')$ is a function of z and z', independent of λ. Typical $f(z,z')$ includes $z+z'+$ constant, $-(z+z')+$ constant, $z-z'+$ constant, $z'-z+$ constant, and $|z-z'|$. When γ_i can be ignored [14], [16], (5) can be simplified as

$$\int_0^\infty \frac{1}{\lambda} e^{-\lambda f(z,z')} \cdot \mathrm{J}_0(\lambda\cdot\Delta\rho)\lambda\, d\,\lambda = 1/\sqrt{\Delta\rho^2+f(z,z')^2}. \tag{6}$$

Comparing (5) and (6), the exponential term is the only difference. However, this exponential term makes the computation much more expensive when calculating the series mutual impedance between two horizontal lines, which is the double integration of (5) or (6) along the source and observation horizontal lines. The analytical expression of the integration of (6) can be found, whereas that of (5) cannot be, i.e., $\int\int 1/\sqrt{(\Delta x_0+y\cot(\phi))^2+(y-y')^2+f(z,z')^2}dy'dy$ is analytically solvable, whereas $\int\int (e^{-\gamma_i\sqrt{(\Delta x_0+y\cot(\phi))^2+(y-y')^2+f(z,z')^2}}/\sqrt{(\Delta x_0+y\cot(\phi))^2+(y-y')^2+f(z,z')^2})dy'dy$ is not.

Fortunately, both the source and observation lines of horizontal wires in 3-D ICs lie on dielectric layers, indicating that (6) instead of (5) can be used (since γ_i in (5) can be ignored).

B. Dilemma in Extraction of v2v and h2v Components of Vector Potential Tensor Green's Functions

The previous subsection illustrates how the DCIM can be efficiently used for h2h series impedance extraction. However, for v2v and h2v, this approach is neither efficient nor necessary, due to the following reasons: 1) if extraction of v2v and h2v needs the same level of accuracy as h2h, the underlying complexity of v2v and h2v is much higher than h2h, since the expressions for v2v and h2v are significantly more complicated; 2) the calculation of the series impedance using the aforementioned method would not be very efficient, since the line integration of (5) instead of (6) is required (due to the fact that the TSVs are embedded within a lossy Si substrate), whereas the analytical expression of the line integration of (5) does not exist; and 3) unlike horizontal wires, TSV height is much smaller than the length of long horizontal wires; therefore, the contribution of TSV series impedance in a circuit is usually not as important as that of long horizontal wires.[3] In other words, TSV is a rather complicated structure that demands less accuracy level than that required for horizontal wires. Can we build some approximate methods, using first-order estimation, to avoid expensive extraction methodologies of TSV series impedance? The answer is affirmative as we illustrate, in detail, in the next few subsections.

III. Approximation and Extraction of v2v and h2v Self and Mutual Series Impedance

Section II-B stated that it is not as efficient to extract the v2v and h2v self and mutual series impedances, if an accurate methodology similar to that for h2h is employed. However, if judicious approximations are made, the v2v and h2v quasi-magnetostatic self and mutual series impedances can be obtained purely analytically. Here, the approximations are justified and explained, and the final analytical expression is obtained.

A. Approximation 1: The Effect of Lower Substrate Is Neglected

Unlike the upper (thin-Si) substrate that surrounds the TSVs, the lower substrate has much weaker influence (via eddy currents) on the TSV series impedance, since it is relatively farther away from the TSVs. For the first-order evaluation of the eddy-current effect on the TSV series impedance, the lower substrate can be neglected. Fig. 3 shows a simplified version of the structure in Fig. 2.

[3]The statement that the horizontal wires can have much larger series impedance than TSVs is relevant to the impedances in real circuits where the horizontal wires can be much longer than TSVs. In the test cases, to demonstrate our TSV impedance model, we will use a wide range of length of the horizontal wires. For example, in Fig. 7, the c2c horizontal wire length d varies from 14 to 50 μm. When $d = 14$ μm, the v2v + h2v impedance is more dominant than the h2h impedance. Therefore, the test cases can capture the error of our v2v + h2v model pretty well.

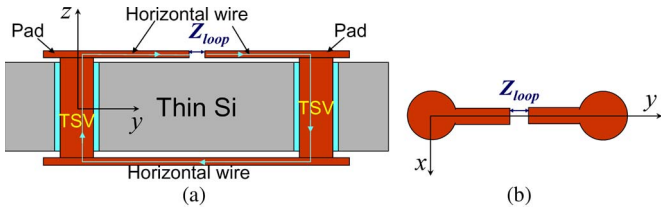

Fig. 3. (a) Cross-sectional view and (b) top view of a TSV horizontal wire loop (without consideration of the lower substrate).

B. Approximation 2: The Total Series Impedance of TSVs Can Be Treated as the Sum of Inner and Outer TSV Impedances, Whereas the Proximity Effect Between Two TSVs Can Be Neglected

When two cylindrical TSVs are close to each other and both of them carry high-frequency current, the current density distribution in one TSV is no longer azimuthal due to the proximity effect. The side effect of azimuthal symmetry break-up is that the inner and outer impedances cannot be separated. However, according to [12], when the c2c distance d between TSVs is six times the TSV radius $r_{\rm TSV}$, the proximity effect can be ignored (as confirmed by the 2D model developed in [11] and [12], which agrees well with a 2D FEM simulator, i.e., Maxwell Student Version (SV) [23]). Since the proximity effect becomes even weaker as d further increases, while the minimum d is around $6r_{\rm TSV}$,[4] the proximity effect can be generally neglected.

The total series impedance of TSVs can be treated as the sum of inner and outer TSV series impedances,[5] i.e.,

$$Z_{\rm TSV} = Z_{\rm inner} + Z_{\rm outer}. \tag{7}$$

Given the high aspect ratio of TSVs, the 2D model in [11] and [12] can be used for the inner series impedance, i.e.,

$$Z_{\rm inner} = \frac{(1-j)\cdot \mathrm{J}_0\left((1-j)r_{\rm TSV}/\delta_{\rm metal}\right)\cdot h_{\rm TSV}}{\sigma_{\rm metal}\cdot 2\pi r_{\rm TSV}\delta_{\rm metal}\cdot \mathrm{J}_1\left((1-j)r_{\rm TSV}/\delta_{\rm metal}\right)} \tag{8}$$

where $\sigma_{\rm metal}$ is the conductivity of TSV metal; $h_{\rm TSV}$ is the TSV height; J_0 and J_1 are the zeroth- and first-order Bessel functions of the first kind, respectively; and $\delta_{\rm metal}$ is the skin depth, i.e.,

$$\delta_{\rm metal} = \sqrt{2/\omega\mu_0\sigma_{\rm metal}}. \tag{9}$$

On the other hand, the 2D model developed in [11] and [12] for the outer series impedance is no longer valid if d is not much smaller than $h_{\rm TSV}$.

[4]The radius of the TSV pad is greater than the TSV itself. Therefore, the minimum d is not around $4r_{\rm TSV}$, but around $6r_{\rm TSV}$.

[5]The outer series impedance has two parts, i.e., the one due to the isolation dielectric and the Si depletion region, and the one due to the Si bulk region. In the following analysis here, we assume a thin dielectric thickness and a small depletion width, but we will include the contribution of isolation dielectric and Si depletion region in Section IV.

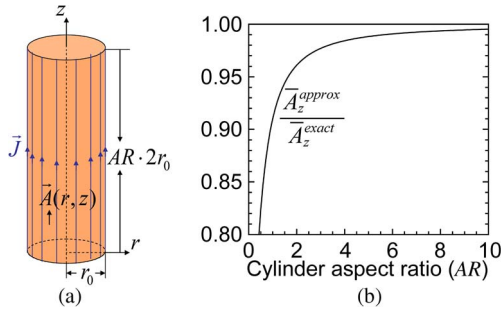

Fig. 4. (a) From a cylinder carrying a uniform z-directional current J_z at the outskirt, one can examine the average z-directional vector potential at the outskirt of a cylinder in free space, the value of which can be obtained either from an exact method or from an approximate method that treats the current as a line current at the center of the cylinder. (b) Ratio of the value from the approximate method to that from the exact method.

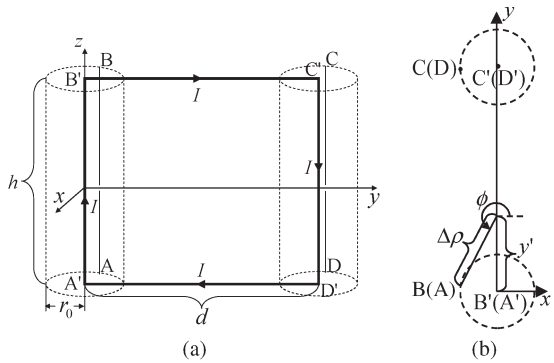

Fig. 5. Schematic overview of two TSVs showing various geometrical parameters used in (11)–(25): (a) the entire view of the structure and (b) the top view.

C. Approximation 3: The Vector Potential Outside a TSV Due to the Current Inside the TSV Can Be Treated as Due to a Line Current at the Center of the TSV

In 2D modeling, this treatment is exact due to the azimuthal symmetry and Ampère's circuital law. To verify the validity of the approximation in 3D, one can examine the average axial directional vector potential $\bar{A}_z$ at the outskirt of a cylinder in free space due to the uniform current (along axial direction) at the outskirt [see the structure shown in Fig. 4(a)]. The ratio of approximate to exact treatment can be expressed as

$$\frac{\bar{A}_z^{\rm approx}}{\bar{A}_z^{\rm exact}} = \frac{\int_0^{AR\cdot 2r_0}\int_0^{AR\cdot 2r_0}\left[1/\sqrt{(z-z')^2+r_0^2}\right]dz'dz}{\int_0^{AR\cdot 2r_0}\int_0^{AR\cdot 2r_0}\int_{-\pi}^{\pi}\frac{1/2\pi}{\sqrt{(z-z')^2+4r_0^2\sin^2\left(\frac{\varphi-\varphi'}{2}\right)}}d\varphi' dz' dz} \tag{10}$$

where AR and r_0 are the aspect ratio and the radius of the cylinder, respectively, and φ' and φ are the angular coordinates of the source and observation points in the cylindrical coordinate system, respectively. The result [shown in Fig. 4(b)] indicates that as long as AR is not too small ($AR > 1.65$), this approximation only induces $< 5\%$ error.

D. Derivation of the TSV Impedances

Given the results in previous subsections, the v2v outer impedance of Fig. 3(a) is approximately the double integral of the source (see lines A′B′ and C′D′ in Fig. 5) and observation points (see lines AB and CD in Fig. 5)

$$\begin{aligned} j\omega L_{\mathrm{v2v}} &= j\omega L^{A}_{\mathrm{v2v}} + j\omega L^{C^{\Phi}}_{\mathrm{v2v}} \\ &\approx 2j\omega\mu_0 \int_{-h/2}^{h/2}\int_{-h/2}^{h/2} \left[G^{A}_{\mathrm{zz}}(r_0,z,z') - G^{A}_{\mathrm{zz}}(d,z,z')\right] dz'dz \\ &\quad + j\omega L^{C^{\Phi}}_{\mathrm{v2v}} \end{aligned} \tag{11}$$[6]

where h is the thickness of the upper substrate surrounding the TSVs;[7] r_0 is the outer radius of the Si depletion region or the isolation dielectric region if the Si depletion region can be neglected ($|\mathrm{A'A}| = |\mathrm{B'B}| = |\mathrm{C'C}| = |\mathrm{D'D}| = r_0$)[7]; d is the c2c distance between the two TSVs ($|\mathrm{A'D'}| = |\mathrm{B'C'}| = d$ and set $|\mathrm{AD'}| = |\mathrm{BC'}| = |\mathrm{A'D}| = |\mathrm{B'C}| = d$); and $L^{C^{\Phi}}_{\mathrm{v2v}}$ is the component due to the C^{Φ} term.

Similarly, the h2v impedance of Fig. 3(a) is approximately the double integral of the source (see lines B′C′ and D′A′ in Fig. 5) and observation points (see lines AB and CD in Fig. 5)

$$\begin{aligned} j\omega M_{\mathrm{h2v}} \approx 2j\omega\mu_0 \int_{-h/2}^{h/2}\int_{0}^{d} &\left[G^{A}_{\mathrm{zy}}(\Delta\rho,\phi,z,h/2)\right. \\ &\left. - G^{A}_{\mathrm{zy}}(\Delta\rho,\phi,z,-h/2)\right] dy'dz \end{aligned} \tag{12}$$

where $\Delta\rho = \sqrt{r_0^2 + y'^2 - r_0^2 y'/d}$, and $\sin(\phi) = (r_0^2/2d - y')/\Delta\rho$, which gives $\sin(\phi)dy' = -d\,\Delta\rho$ and

$$\begin{aligned} j\omega M_{\mathrm{h2v}} \approx 2j\omega\mu_0 \int_{-h/2}^{h/2}\int_{r_0}^{d} -\frac{1}{\sin(\phi)} &\left[G^{A}_{\mathrm{zy}}(\Delta\rho,\phi,z,h/2)\right. \\ &\left. - G^{A}_{\mathrm{zy}}(\Delta\rho,\phi,z,-h/2)\right] d\,\Delta\rho\,dz. \end{aligned} \tag{13}$$

It is easy to prove the following relationship among the outer series impedances of v2v (due to C^{Φ}), h2v, and v2h, i.e.,

$$-L^{C^{\Phi}}_{\mathrm{v2v}} = M_{\mathrm{h2v}} = M_{\mathrm{v2h}}. \tag{14}$$

Therefore, $L^{C^{\Phi}}_{\mathrm{v2v}}$ and M_{v2h} always cancel out, and they are consequently not considered in the following paragraphs.

By changing the integration order, (3b) and (11) give

$$\begin{aligned} j\omega L^{A}_{\mathrm{v2v}} \approx \frac{j\omega\mu_0}{\pi} \int_0^{\infty} &\left[\mathrm{J}_0(\lambda r_0) - \mathrm{J}_0(\lambda\, d)\right] \lambda \\ &\cdot \int_{-h/2}^{h/2}\int_{-h/2}^{h/2} \tilde{G}^{A}_{\mathrm{zz}}(\lambda,z,z')dz'dzd\,\lambda. \end{aligned} \tag{15}$$

Similarly, (3d) and (13) give

$$\begin{aligned} j\omega M_{\mathrm{h2v}} \approx \frac{\omega\mu_0}{\pi} \int_0^{\infty} &\left[\mathrm{J}_0(\lambda r_0) - \mathrm{J}_0(\lambda\, d)\right] \\ &\cdot \int_{-h/2}^{\frac{h}{2}} \left[\tilde{G}^{A}_{\mathrm{zu}}(\lambda,z,-h/2) - \tilde{G}^{A}_{\mathrm{zu}}(\lambda,z,h/2)\right] dzd\,\lambda. \end{aligned} \tag{16}$$

The spectral-domain vector potential Green's function $\tilde{G}^{A}_{\mathrm{zz}}$ and $\tilde{G}^{A}_{\mathrm{zu}}$ can be obtained from the transmission line Green's functions of layered media [21],[8] and the $dz'dz$ integral in (15) can be expressed as

$$\begin{aligned} \tilde{G}^{A}_{\mathrm{zz,int}} &= \int_{-h/2}^{h/2}\int_{-h/2}^{h/2} \tilde{G}^{A}_{\mathrm{zz}}(\lambda,z,z')dz'dz \\ &= \frac{e^{-m_0 h} - 1 + m_0 h}{m_0^3} - \frac{(1-e^{-m_0 h})^2}{(1+e^{-m_0 h})m_0^3} \end{aligned} \tag{17}$$

and the dz integral in (16) can be expressed in (18), shown at the bottom of the next page, where $m_0(\lambda) = \sqrt{\lambda^2 + j\omega\mu_0\sigma_{\mathrm{Si}}}$, and σ_{Si} is the complex effective conductivity of Si. In (17), the first term on the right-hand side is due to the "source," which represents the value if the TSVs are surrounded by a homogeneous Si substrate

$$\tilde{G}^{A,\mathrm{source}}_{\mathrm{zz,int}} = \tilde{G}^{A,\mathrm{homogeneous\,sub}}_{\mathrm{zz,int}} = (e^{-m_0 h} - 1 + m_0 h)/m_0^3 \tag{19}$$

while the second term is due to the "images," i.e., the reflections at the boundaries of layered media.

It should be noted that when $\omega \to 0$, $\tilde{G}^{A}_{\mathrm{zz,int}}$ itself does not reduce to the free-space value ($\tilde{G}^{A,\mathrm{free\,space}}_{\mathrm{zz,int}}$), where

$$\tilde{G}^{A,\mathrm{free\,space}}_{\mathrm{zz,int}} = (e^{-\lambda h} - 1 + \lambda h)/\lambda^3. \tag{20}$$

However, this is not against physical laws because when $\omega \to 0$, $\tilde{G}^{A}_{\mathrm{zz,int}} - j\tilde{G}^{A}_{\mathrm{zu,int}}/\lambda \to (e^{-\lambda h} - 1 + \lambda h)/\lambda^3$. The implication from the asymptotic behavior of $\tilde{G}^{A}_{\mathrm{zz,int}}$ and $\tilde{G}^{A}_{\mathrm{zu,int}}$ is that the

[6]The entire equation of (11) represents the total v2v outer impedance between two TSVs, i.e., the integration of $G^{A}_{\mathrm{zz}}(r_0,z,z')$ represents the self term, whereas that of $G^{A}_{\mathrm{zz}}(d,z,z')$ represents the mutual term. The $G^{A}_{\mathrm{zz}}(r_0,z,z')$ related term (self-term) originates from the vector potential at the cylindrical TSV shell due to a unit current inside TSV, which is approximately independent of the current distribution inside TSV, as long as the approximations in Sections III-B and III-C are valid. Therefore, we can use the integration of $G^{A}_{\mathrm{zz}}(r_0,z,z')$, which is the vector potential due to a unit current source at the TSV center line, to represent the vector potential due to a unit current with distribution inside TSV. A similar expression can be found in [8]: if a TSV is in the free space (no substrate surrounding it), the self-inductance is reduced to (8) in [8]; if excluding the $h/4$ term, (8) in [8] represents the self-outer inductance.

[7]Here, we assume that both the horizontal wires are very close to the upper substrate, implying that $h_{\mathrm{TSV}} \approx h$; we also assume that the TSV radius $r_{\mathrm{TSV}} \approx r_0$. In real situations, h_{TSV} is slightly greater than h, whereas $r_0 > r_{\mathrm{TSV}}$. These effects will be considered in (34)–(37) in the Appendix and in Section IV.

[8]Due to the limitation of page numbers, detailed derivations of the spectral-domain vector potential Green's functions are not shown in this paper.

partial impedances themselves are not physical, but the loop impedance is physical (physically, in a quasi-magnetostatic approach, a segment of current cannot exist by itself, but the current always forms a loop).

E. Approximation 4: First-Order Analytical Model for TSV Impedances

From (15)–(18), the v2v + h2v TSV impedance, i.e., $j\omega L^A_{\rm v2v} + j\omega M_{\rm h2v}$, can be obtained. However, the calculation using these equations is not efficient. This is because the $d\lambda$ integrations in (15) and (16) are not analytical, whereas the numerical $d\lambda$ integration requires an evaluation of Bessel functions of a wide range of λ. Fortunately, first-order approximations can be made.

The first-order expression of $\tilde{G}^A_{\rm zz,int} - j\tilde{G}^A_{\rm zu,int}/\lambda - \tilde{G}^{A,\rm free\,space}_{\rm zz,int}$ can be obtained from the following steps: make a Taylor series of $(17) - (j/\lambda) * (18) - (20)$ at $\omega = 0$ and ignore $O(\omega^2)$; apply function "ln" and make a series at $\lambda = 0$ and ignore $O(\lambda^2)$; apply function "exp." The result is expressed as

$$\tilde{G}^A_{\rm zz,int} - \frac{j\tilde{G}^A_{\rm zu,int}}{\lambda} - \tilde{G}^{A,\rm free\,space}_{\rm zz,int} \approx -\frac{jh^4\omega\mu_0\sigma_{\rm Si}}{12}\frac{1}{\lambda}\exp\left(-\frac{13}{20}\lambda h\right). \quad (21)$$

The approximation is valid as long as the frequency is not too high. A rule of thumb requires that the damping parameter in silicon $\delta_{\rm Si}$ satisfies

$$\delta_{\rm Si} = \sqrt{2/\omega\mu_0\sigma_{\rm Si}} > h/2. \quad (22)$$

From (15)–(21) and utilizing the integration of (6)

$$\begin{aligned} j\omega L^A_{\rm v2v} + j\omega M_{\rm h2v} &\approx \frac{j\omega\mu_0}{\pi}\cdot\left[r_0 + h\,\mathrm{arcsinh}(h/r_0) - \sqrt{r_0^2+h^2}\right] \\ &\quad - \frac{j\omega\mu_0}{\pi}\cdot\left[d + h\,\mathrm{arcsinh}(h/d) - \sqrt{d^2+h^2}\right] \\ &\quad + \frac{h^4\omega^2\mu_0^2\sigma_{\rm Si}}{12\pi}\left(r_0^2 + \frac{169}{400}h^2\right)^{-1/2} \\ &\quad - \frac{h^4\omega^2\mu_0^2\sigma_{\rm Si}}{12\pi}\left(d^2 + \frac{169}{400}h^2\right)^{-1/2} \end{aligned} \quad (23)$$

which is a purely analytical expression. The expression implies that the outer series TSV impedance can be treated as two separate parts, i.e., $R_{\rm sub}$ (the resistance due to substrate eddy currents) and $j\omega L_{\rm outer}$ ($L_{\rm outer}$ is the outer inductance), where

$$R_{\rm sub} \approx \frac{h^4\omega^2\mu_0^2\sigma_{\rm Si}}{12\pi}\left(r_0^2 + \frac{169}{400}h^2\right)^{-1/2} - \frac{h^4\omega^2\mu_0^2\sigma_{\rm Si}}{12\pi}\left(d^2 + \frac{169}{400}h^2\right)^{-1/2} \quad (24)$$

and

$$\begin{aligned} j\omega L_{\rm outer} &\approx \frac{j\omega\mu_0}{\pi}\cdot\left[r_0 + h\,\mathrm{arcsinh}(h/r_0) - \sqrt{r_0^2+h^2}\right] \\ &\quad - \frac{j\omega\mu_0}{\pi}\cdot\left[d + h\,\mathrm{arcsinh}(h/d) - \sqrt{d^2+h^2}\right]. \end{aligned} \quad (25)$$

In addition, $L_{\rm outer}$ is independent of frequency in first order.

The accuracy of (23) is verified by comparing its calculation results with the results from (15)–(18). The results are shown in Fig. 6, which illustrates the following statements: 1) While the surrounding substrate greatly reduces the $L_{\rm outer}$ in the 2D case and in 3D homogeneous case, it does not have much effect on layered substrate. This is because in layered substrate, the finite Si thickness makes the impact of substrate eddy currents on $L_{\rm outer}$ second-order effect; 2) v2v itself does not reduce to the case for free space, which is in agreement with the discussion in the previous subsection; 3) The first-order approximation gives reasonably good result in the frequency range up to 100 GHz with different c2c TSV distances. The small deviation at high frequencies and large c2c distance is tolerable, since the significant frequency for large distance signal transport is also lower.

IV. Verification Against Full-Wave Simulation

The impedance in a real 3-D structure includes the v2v + h2v TSV series impedance, which is discussed in Section III; the h2h horizontal wire series impedance, which is discussed in Section II-A; and the capacitance values. As an example, the

$$\tilde{G}^A_{\rm zu,int} = \int_{-h/2}^{h/2}\left[\tilde{G}^A_{\rm zu}(\lambda,z,-h/2) - \tilde{G}^A_{\rm zu}(\lambda,z,h/2)\right]dz = \frac{2j\left[(m_0+\lambda)+(\lambda-m_0)e^{-m_0h}\right]\left(1-e^{-m_0h}\right)^2}{m_0\cdot(m_0+\lambda)^2(1+e^{-m_0h}) - m_0\cdot(m_0-\lambda)^2(1+e^{-m_0h})e^{-2m_0h}} \quad (18)$$

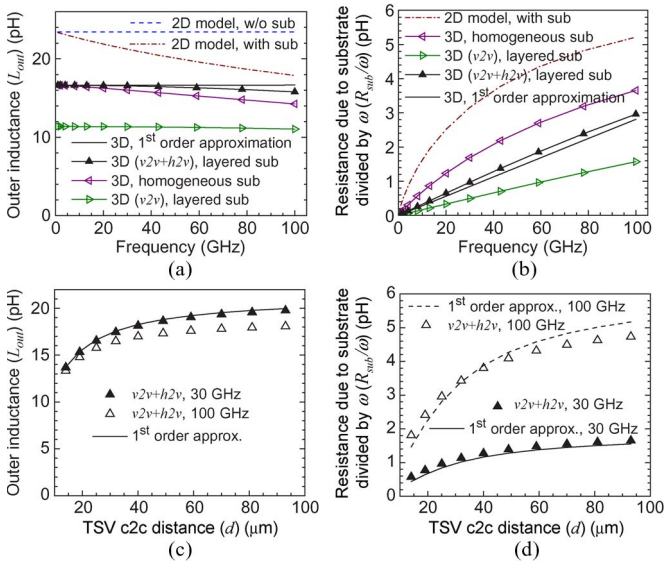

Fig. 6. TSV outer series impedance from different models: (a) $L_{\rm out}$ versus frequency; (b) $R_{\rm sub}/\omega$ versus frequency; (c) $L_{\rm out}$ versus d; and (d) $R_{\rm sub}/\omega$ versus d. The data labeled as "3D (v2v + h2v), layered sub" or simply "v2v + h2v" are obtained from (15)–(18); the data labeled as "3D, 1st order approximation" or simply "1st order approx." are obtained from (23); the data labeled as "3D, v2v, layered sub" are obtained from (15) and (17); the data labeled as "3D, homogeneous sub" are obtained from (15) and (19); and the data labeled as "2D model, w/o sub" and "2D model, with sub" are obtained from the 2D model in [12]. Note that all the labeling of v2v has not considered the C^{Φ} term. The material and geometrical properties used are $\sigma_{\rm Si} = 10^4$ S/m; $h = 25$ μm; $r_0 = 2.4$ μm; and for (a) and (b), $d = 25$ μm.

equivalent circuit of a typical structure (see Fig. 7(a)[9]) is shown in Fig. 7(b).

In the structure, the h2h series impedance can be obtained from the quasi-magnetostatic DCIM approximation. Here, an equivalent rectangular wire with length $= d$ (c2c pad distance) and effective wire width $w_{\rm eff}$ is used so that the DC resistance of the horizontal wires is maintained

$$\begin{aligned}\frac{d}{\sigma_{\rm wire} w_{\rm eff} t_{\rm wire}} &= R_{\rm DC,horizontal} \\ &= R_{\rm DC,rectangular\,wire} + 2R_{\rm DC,pad} \\ &= \frac{d - 2\sqrt{r_{\rm pad}^2 - (w_{\rm wire}/2)^2}}{\sigma_{\rm wire} w_{\rm wire} t_{\rm wire}} \\ &\quad + \frac{2}{\sigma_{\rm wire} t_{\rm wire}} \int_0^{\sqrt{r_{\rm pad}^2 - (w_{\rm wire}/2)^2}} \frac{1}{2\sqrt{r_{\rm pad}^2 - y^2}} dy\end{aligned} \tag{26}$$

[9]The loop structures that we have studied are just for test purpose, i.e., to verify our model, whereas our model is valid for any circuit configuration. Our paper illustrates that the "partial impedance" approach (see the Appendix) is valid for both TSVs and horizontal wires: one can separate different components of interconnects (including both TSVs and horizontal wires) and build up the circuit model from the partial impedances. However, to verify our model, a closed loop must be used because "partial impedance" does not have a physical meaning itself, unless a loop is formed. In addition, there is always a return current path for any "signal path." For example, to transfer the signal from one chip to another through a TSV, the V_{DD} or Gnd TSVs will serve as the return path. In other words, a loop is always there.

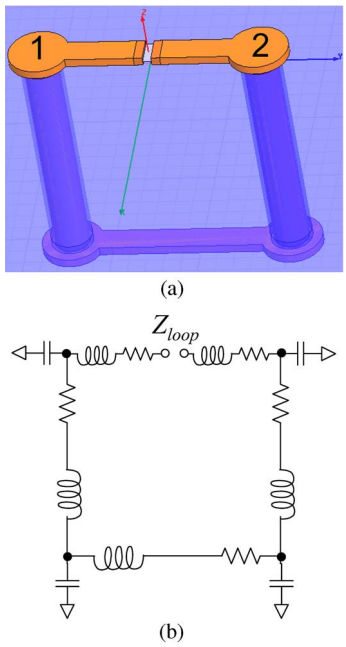

Fig. 7. (a) A typical structure with two TSVs and two horizontal wires and (b) its equivalent circuit. Thin Si (upper substrate) thickness is 25 μm; lower substrate thickness is 500 μm; both Si substrates have resistivity of 0.01 $\Omega \cdot$ cm (depletion region can be neglected in such low resistivity or highly doped Si); a 10-μm SiO_2 layer is in between the Si substrates; a 1-μm SiO_2 layer is on top of the upper Si substrate; the c2c distance d between Cu TSVs (2.2 $\mu\Omega \cdot$ cm) varies 14, 25, and 50 μm; TSV metal has a diameter of 4 μm; TSV isolation dielectric is 0.4 μm SiO_2; the Cu horizontal wires (2.2 $\mu\Omega \cdot$ cm) have 1-μm height and 1.5-μm distance from the wire center to the upper Si substrate surface (which indicates c2c TSV height of 28 μm), including 3-μm-width rectangular wires and 7-μm-diameter pads (from (27), $w_{\rm eff}$ varies from 3.80, 3.40, and 3.19 μm when d varies from 14, 25, and 50 μm, respectively).

where $r_{\rm pad}$ is the radius of TSV pads; and $t_{\rm wire}$, $w_{\rm wire}$, and $\sigma_{\rm wire}$ are the thickness, width, and conductivity of the horizontal wires, respectively. From (26)

$$w_{\rm eff} = w_{\rm wire} \cdot \frac{d}{d - 2\sqrt{r_{\rm pad}^2 - (w_{\rm wire}/2)^2} + w_{\rm wire} \arccos(w_{\rm wire}/2r_{\rm pad})}. \tag{27}$$

The v2v + h2v series impedance can be obtained from the methodology developed in Section III-E. The outer series impedance of the whole loop (including both v2v and h2v components) to TSV 1 in Fig. 7(a) can be obtained from (34) and (35) with $n = 1$ (see the Appendix). Note that $h_{\rm TSV}$ instead of h and $r_{\rm TSV}$ instead of r_0 should be used in (35) because of the different boundaries of TSV metal and the Si bulk region. The inner series impedance of the TSVs can be obtained from (8).

In addition to the series impedances, the capacitance values are also required for the final loop impedance extraction, where their contribution becoming important as the frequency increases. Due to the low resistivity of the Si substrate in the example in Fig. 7, the Si substrate can be treated as a good ground conductor for capacitance extraction. In this situation, 2D capacitance models or simulations are good enough, since all the wires and TSVs are close to the substrate surface. In this

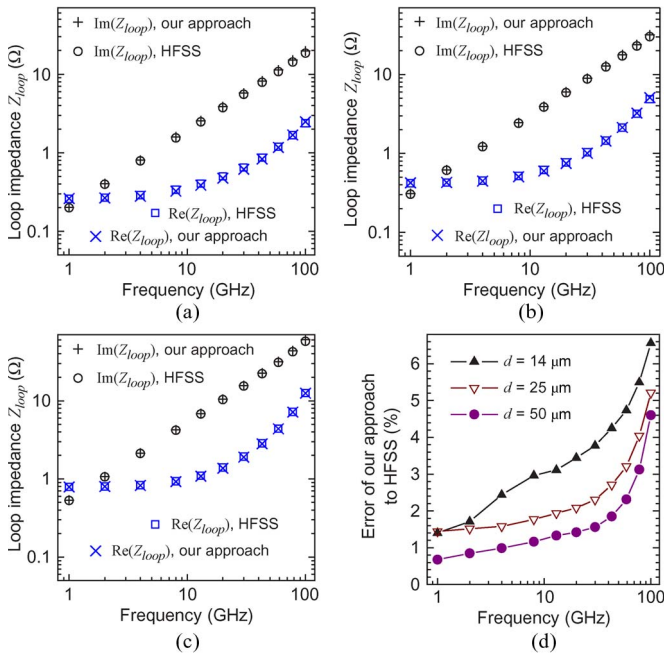

Fig. 8. Loop impedance $Z_{\rm loop}$ of the structure shown in Fig. 7(a) from both our approach and HFSS [20] with various c2c distances d between TSVs: (a) $d = 14$ μm; (b) $d = 25$ μm; and (c) $d = 50$ μm. (d) Relative error of our approach against the HFSS result with various d's, where the relative error is defined as $|Z_{\rm loop}^{\rm our\ approach} - Z_{\rm loop}^{\rm HFSS}|/|Z_{\rm loop}^{\rm HFSS}|$.

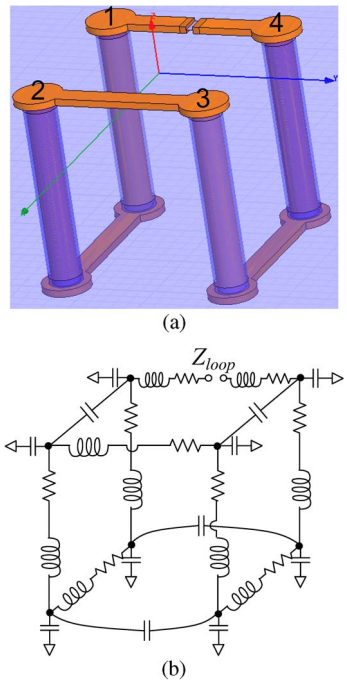

Fig. 9. (a) Typical structure with four TSVs and four horizontal wires and (b) its equivalent circuit. The stack information (geometrical and material information of the substrates) and interconnect information (z-coordinates, height, width, and pad size of horizontal wires; diameter and isolation dielectric of TSVs; and metal conductivity) are the same as in Fig. 7. The Cu TSVs form a square from top view, with a c2c distance between neighbor TSVs of 25 μm; from (27), the Cu horizontal wires have an effective width of $w_{\rm eff} = 3.40$ μm.

paper, Maxwell SV [23] is used to extract the capacitance of horizontal wires, whereas the 2D cylindrical capacitance model in [11] and [12] is used to calculate the TSV capacitance.

With the series impedances and capacitance values of each segments and the equivalent circuit shown in Fig. 7(b), the loop impedance can be obtained. Our calculation results are compared with a rigorous FEM-based EM solver HFSS [20] (see Fig. 8). Within the frequency range, our approach shows $< 7\%$ error as compared to HFSS.

Although a single loop (as in Fig. 5) is assumed when developing the approach, the approach is valid for more complicated structures like the one in Fig. 9(a)[9]. The reason is explained in the Appendix. The outer series impedance of the whole loop (including both v2v and h2v components) to TSV 1 in Fig. 7(a) can be obtained from (34) and (35) with $n = 2$ (see the Appendix).

Using the equivalent circuit shown in Fig. 9(b), the loop impedance can be obtained. Within the frequency range, our approach shows $< 6\%$ error, as compared to HFSS [20] (see Fig. 10).

The steps for impedance extraction of TSVs and horizontal interconnects are summarized in Fig. 11. Note that the series impedances related to TSVs are extracted from purely analytical equations.

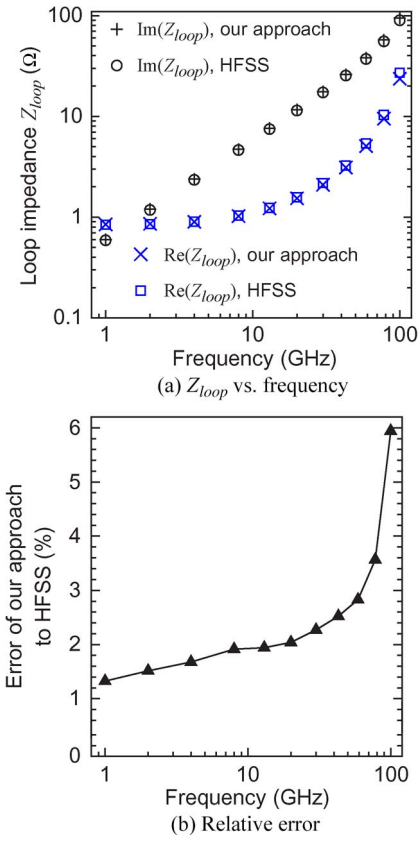

Fig. 10. (a) Loop impedance $Z_{\rm loop}$ of the structure shown in Fig. 9(a) from both our approach and HFSS [20]; (b) relative error of our approach against the HFSS result (the definition of the relative error is the same as in Fig. 8).

V. Summary

In this paper, the series impedances of both the horizontal wires and TSVs in 3-D ICs are investigated. A physical model with analytical expressions with first-order approximation for the TSV series impedance is developed from v2v and h2v

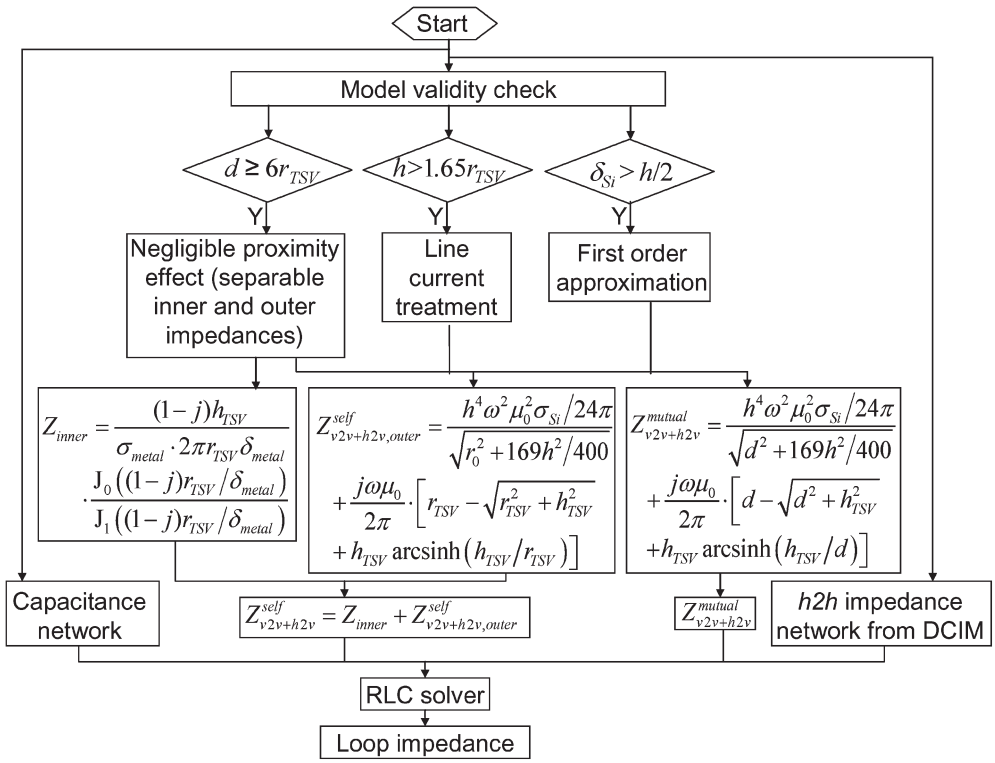

Fig. 11. Flowchart of loop impedance extraction with both TSVs and horizontal interconnects in 3-D IC.

vector potential Green's functions. The first-order approximation shows good accuracy in the entire range of interest of both the frequency and the c2c distance between TSVs. Along with the contribution of horizontal wire series impedances (extracted from DCIM), as well as the capacitance values of TSVs and horizontal wires, the total impedance is obtained from an RLC equivalent circuit. The calculation results of our approach are contrasted against the full-wave FEM EM solver HFSS, resulting in maximum deviations smaller than 7% in the frequency range of interest. Our methodology is attractive for system-level interconnect impedance extraction in 3-D ICs that is critical for the performance evaluation and design optimization of 3-D ICs.

APPENDIX
MATHEMATICAL INDUCTION PROOF TO DEMONSTRATE THAT OUR APPROACH (COMBINING h2v AND v2v IMPEDANCES) CAN BE USED IN COMPLICATED WIRE LOOPS

The mathematical induction proof starts from the simplest wire loop, which contains two TSVs and two horizontal wires, as shown in Fig. 12(a). In the structure of Fig. 12(a), from (15), we can define the v2v partial outer series impedance function $Z^{\mathrm{partial}}_{\mathrm{v2v}}(r)$ so that

$$j\omega L^{A}_{\mathrm{v2v}} \approx 2\left(Z^{\mathrm{partial}}_{\mathrm{v2v}}(r_0) - Z^{\mathrm{partial}}_{\mathrm{v2v}}(d)\right). \tag{28}$$

Similarly, from (16), we can define the h2v partial outer series impedance function $Z^{\mathrm{partial}}_{\mathrm{upper\_h2v}}(r_1, r_2)$ (for upper horizontal wire to TSV interaction) and $Z^{\mathrm{partial}}_{\mathrm{lower\_}h2v}(r_1, r_2)$ (for lower horizontal wire to TSV interaction) so that

$$j\omega M_{\mathrm{h2v}} \approx 2\left(Z^{\mathrm{partial}}_{\mathrm{upper\_h2v}}(r_0, d) - Z^{\mathrm{partial}}_{\mathrm{lower\_h2v}}(r_0, d)\right). \tag{29}$$[10]

In addition, we can define functions $f_{\mathrm{upper\_h2v}}(r)$ and $f_{\mathrm{lower\_h2v}}(r)$ so that

$$\begin{cases} Z^{\mathrm{partial}}_{\mathrm{upper\_h2v}}(r_1, r_2) = f_{\mathrm{upper\_h2v}}(r_1) - f_{\mathrm{upper\_h2v}}(r_2) \\ Z^{\mathrm{partial}}_{\mathrm{lower\_h2v}}(r_1, r_2) = f_{\mathrm{lower\_h2v}}(r_1) - f_{\mathrm{lower\_h2v}}(r_2) \end{cases}. \tag{30}$$

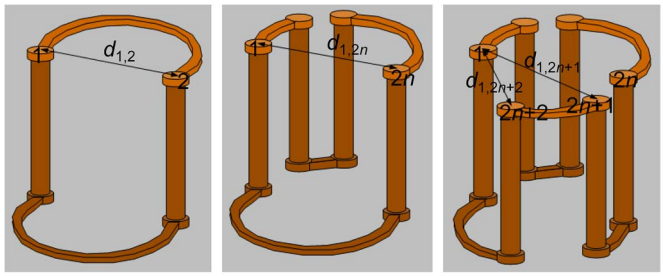

Fig. 12. Schematic figures during the mathematical induction proof; as we prove (a) the most simple case (wire loop with two TSVs and two horizontal wires) and the recurrence relation from (b) the case of wire loop with $2n$ TSVs and $2n$ horizontal wires to (c) the case of wire loop with $2n+2$ TSVs and $2n+2$ horizontal wires, we demonstrate that combining v2v and h2v loop outer series impedances [see (24) and (25)] is valid for any wire loop.

[10]Note that (16) is valid for horizontal wires of any arbitrary curve, not necessarily straight lines. This can be derived by replacing dy' with dl' (the curve integration variable) in the integral of (12) and following the same derivation steps of (12) → (13) → (16).

For the simplest wire loop (two TSVs and two horizontal wires), if we can consider the impact of the entire loop, including the TSVs and horizontal wires on TSV 1 [see Fig. 12(a)], the total v2v self and mutual outer series impedance can be expressed as

$$Z_{\mathrm{v2v}}^{\mathrm{all\_to\_1}} \approx Z_{\mathrm{v2v}}^{\mathrm{partial}}(r_0) - Z_{\mathrm{v2v}}^{\mathrm{partial}}(d_{1,2}) \tag{31a}$$

where $d_{\eta,\nu}$ is the c2c distance between TSV η and ν. The total h2v mutual outer series impedance can be expressed as

$$\begin{aligned} Z_{\mathrm{h2v}}^{\mathrm{all\_to\_1}} &\approx Z_{\mathrm{upper\_h2v}}^{\mathrm{partial}}(r_0, d_{1,2}) - Z_{\mathrm{lower\_h2v}}^{\mathrm{partial}}(r_0, d_{1,2}) \\ &= f_{\mathrm{upper\_h2v}}(r_0) - f_{\mathrm{upper\_h2v}}(d_{1,2}) \\ &\quad - \left(f_{\mathrm{lower\_h2v}}(r_0) - f_{\mathrm{lower\_h2v}}(d_{1,2})\right). \end{aligned} \tag{31b}$$

Note the similarity of (31a) and (31b): both of them can be expressed as $\mathrm{func}(r_0) - \mathrm{func}(d_{1,2})$, where $\mathrm{func}(r)$ can be either $Z_{\mathrm{v2v}}^{\mathrm{partial}}(r)$ or $f_{\mathrm{upper\_h2v}}(r) - f_{\mathrm{lower\_h2v}}(r)$.

Now, if for a wire loop with $2n$ TSVs and $2n$ horizontal wires, the total v2v self and mutual, as well as h2v mutual outer series impedances, can be expressed as a similar form, i.e.,

$$\begin{aligned} Z_{\mathrm{v2v}}^{\mathrm{all\_to\_1}} &\approx Z_{\mathrm{v2v}}^{\mathrm{partial}}(r_0) + \sum_{\nu=2}^{n} Z_{\mathrm{v2v}}^{\mathrm{partial}}(d_{1,2\nu-1}) \\ &\quad - \sum_{\nu=1}^{n} Z_{\mathrm{v2v}}^{\mathrm{partial}}(d_{1,2\nu}) \end{aligned} \tag{32a}$$

$$\begin{aligned} Z_{\mathrm{h2v}}^{\mathrm{all\_to\_1}} &\approx f_{\mathrm{upper\_h2v}}(r_0) + \sum_{\nu=2}^{n} f_{\mathrm{upper\_h2v}}(d_{1,2\nu-1}) \\ &\quad - \sum_{\nu=1}^{n} f_{\mathrm{upper\_h2v}}(d_{1,2\nu}) \\ &\quad - \left[f_{\mathrm{lower\_h2v}}(r_0) + \sum_{\nu=2}^{n} f_{\mathrm{lower\_h2v}}(d_{1,2\nu-1}) \right. \\ &\qquad \left. - \sum_{\nu=1}^{n} f_{\mathrm{lower\_h2v}}(d_{1,2\nu}) \right] \end{aligned} \tag{32b}$$

where we can derive the case of a wire loop with $2n+2$ TSVs and $2n+2$ horizontal wires, by breaking the last horizontal wire (from the $2n$th TSV to the first TSV) into three horizontal wires and two TSVs [see Fig. 12(b) and (c)]. Obviously, the total v2v self and mutual outer series impedance can be expressed as

$$\begin{aligned} Z_{\mathrm{v2v}}^{\mathrm{all\_to\_1}} &\approx Z_{\mathrm{v2v}}^{\mathrm{partial}}(r_0) + \sum_{\nu=2}^{n+1} Z_{\mathrm{v2v}}^{\mathrm{partial}}(d_{1,2\nu-1}) \\ &\quad - \sum_{\nu=1}^{n+1} Z_{\mathrm{v2v}}^{\mathrm{partial}}(d_{1,2\nu}). \end{aligned} \tag{33a}$$

The total h2v mutual outer series impedance can be derived as

$$\begin{aligned} Z_{\mathrm{h2v}}^{\mathrm{all\_to\_1}} &\approx f_{\mathrm{upper\_h2v}}(r_0) + \sum_{\nu=2}^{n} f_{\mathrm{upper\_h2v}}(d_{1,2\nu-1}) \\ &\quad - \sum_{\nu=1}^{n} f_{\mathrm{upper\_h2v}}(d_{1,2\nu}) \\ &\quad - \left[f_{\mathrm{lower\_h2v}}(r_0) + \sum_{\nu=2}^{n} f_{\mathrm{lower\_h2v}}(d_{1,2\nu-1}) \right. \\ &\qquad \left. - \sum_{\nu=1}^{n} f_{\mathrm{lower\_h2v}}(d_{1,2\nu}) \right] \\ &\quad + Z_{\mathrm{lower\_h2v}}^{\mathrm{partial}}(r_0, d_{1,2n}) - Z_{\mathrm{lower\_h2v}}^{\mathrm{partial}}(r_0, d_{1,2n+2}) \\ &\quad + Z_{\mathrm{upper\_h2v}}^{\mathrm{partial}}(d_{1,2n+1}, d_{1,2n+2}) \\ &\quad - Z_{\mathrm{lower\_h2v}}^{\mathrm{partial}}(d_{1,2n+1}, d_{1,2n}) \\ &= f_{\mathrm{upper\_h2v}}(r_0) + \sum_{\nu=2}^{n+1} f_{\mathrm{upper\_h2v}}(d_{1,2\nu-1}) \\ &\quad - \sum_{\nu=1}^{n+1} f_{\mathrm{upper\_h2v}}(d_{1,2\nu}) \\ &\quad - \left[f_{\mathrm{lower\_h2v}}(r_0) + \sum_{\nu=2}^{n+1} f_{\mathrm{lower\_h2v}}(d_{1,2\nu-1}) \right. \\ &\qquad \left. - \sum_{\nu=1}^{n+1} f_{\mathrm{lower\_h2v}}(d_{1,2\nu}) \right]. \end{aligned} \tag{33b}$$

From (31a) and (31b), which states the validity of the simplest case (two TSVs and two horizontal wires), and the recurrence relation from (32a) and (32b) ($2n$ TSVs and $2n$ horizontal wires) to (33a) and (33b) ($2n+2$ TSVs and $2n+2$ horizontal wires), we can state that for any wire loops with $2n$ TSVs and $2n$ horizontal wires [see Fig. 12(b)], $Z_{\mathrm{v2v}}^{\mathrm{all\_to\_1}}$ and $Z_{\mathrm{h2v}}^{\mathrm{all\_to\_1}}$ have the similar expression of $\mathrm{func}(r_0) + \sum_{\nu=2}^{n} \mathrm{func}(d_{1,2\nu-1}) - \sum_{\nu=1}^{n} \mathrm{func}(d_{1,2\nu})$.

Therefore, not only v2v but also h2v contributions can be reduced to the series impedances among TSVs, regardless of how the loop is formed (i.e., how the horizontal wires are used to form the loop). The approach developed in Section III-E, particularly (24) and (25), can be used for v2v + h2v series impedance extraction for any wire loops with $2n$ TSVs and $2n$ horizontal wires [see Fig. 12(b)]. Therefore, the outer series impedance of the whole loop to TSV 1 can be expressed as

$$\begin{aligned} &\mathrm{Re}\left(Z_{\mathrm{v2v}}^{\mathrm{all\_to\_1}} + Z_{\mathrm{h2v}}^{\mathrm{all\_to\_1}}\right) \\ &\approx \frac{h^4\omega^2\mu_0^2\sigma_{Si}}{24\pi} \\ &\quad \cdot \left[\left(r_0^2 + \frac{169}{400}h^2\right)^{-1/2} + \sum_{\nu=2}^{n} \left(d_{1,2\nu-1}^2 + \frac{169}{400}h^2\right)^{-1/2} \right. \\ &\qquad \left. - \sum_{\nu=1}^{n} \left(d_{1,2\nu}^2 + \frac{169}{400}h^2\right)^{-1/2} \right] \end{aligned} \tag{34}$$

$$\begin{aligned} &j\mathrm{Im}\left(Z_{\mathrm{v2v}}^{\mathrm{all\_to\_1}} + Z_{\mathrm{h2v}}^{\mathrm{all\_to\_1}}\right) \\ &\approx j\omega\mu_0/2\pi \cdot \left[r_{\mathrm{TSV}} + h_{\mathrm{TSV}} \operatorname{arcsinh}(h_{\mathrm{TSV}}/r_{\mathrm{TSV}}) \right. \\ &\qquad \left. - \sqrt{r_{\mathrm{TSV}}^2 + h_{\mathrm{TSV}}^2} \right] \\ &\quad + j\omega\mu_0/2\pi \cdot \sum_{\nu=2}^{n} \left[d_{1,2\nu-1} + h_{\mathrm{TSV}} \operatorname{arcsinh}(h_{\mathrm{TSV}}/d_{1,2\nu-1}) \right. \\ &\qquad \left. - \sqrt{d_{1,2\nu-1}^2 + h_{\mathrm{TSV}}^2} \right] \\ &\quad - j\omega\mu_0/2\pi \cdot \sum_{\nu=1}^{n} \left[d_{1,2\nu} + h_{\mathrm{TSV}} \operatorname{arcsinh}(h_{\mathrm{TSV}}/d_{1,2\nu}) \right. \\ &\qquad \left. - \sqrt{d_{1,2\nu}^2 + h_{\mathrm{TSV}}^2} \right]. \end{aligned} \tag{35}$$

Note that $h_{\rm TSV}$ instead of h and $r_{\rm TSV}$ instead of r_0 are used in (35) because of the different boundaries of TSV metal and the Si bulk region. Equations (34) and (35) can be extended to the case of mutual v2v + h2v series impedance extraction between two wire loops, i.e.,

$$\begin{aligned}&{\rm Re}\left(Z_{v2v+h2v}^{\rm loop\_a\_to\_b}\right)\\&\quad\approx\frac{h^4\omega^2\mu_0^2\sigma_{\rm Si}}{24\pi}\cdot\sum_{\eta=1}^{2m}\sum_{\nu=1}^{2n}(-1)^{\nu+\eta}\left(d_{b(\eta),a(\nu)}^2+\frac{169}{400}h^2\right)^{-1/2}\end{aligned}\tag{36}$$

$$\begin{aligned}&j{\rm Im}\left(Z_{v2v+h2v}^{\rm loop\_a\_to\_b}\right)\\&\quad\approx j\omega\mu_0/2\pi\cdot\sum_{\eta=1}^{2m}\sum_{\nu=1}^{2n}\\&\qquad(-1)^{\nu+\eta}\left[d_{b(\eta),a(\nu)}+h_{\rm TSV}\,{\rm arcsinh}\left(\frac{h_{\rm TSV}}{d_{b(\eta),a(\nu)}}\right)\right.\\&\qquad\left.-\sqrt{d_{b(\eta),a(\nu)}^2+h_{\rm TSV}^2}\right]\end{aligned}\tag{37}$$

where the two loops are named "a" and "b," which contain $2n$ and $2m$ TSVs, respectively; and $d_{b(\eta),a(\nu)}$ is the c2c distance between the ηth TSV in loop b and the νth TSV in loop a. Note that if $d_{b(\eta),a(\nu)}=0$ exists [if loop a and b share TSV(s)], the corresponding $d_{b(\eta),a(\nu)}$ should be replaced with r_0 in (36) and $r_{\rm TSV}$ in (37), respectively, and TSV inner impedance should be added.

REFERENCES

[1] K. Banerjee, S. J. Souri, P. Kapur, and K. C. Saraswat, "3-D ICs: A novel chip design for improving deep-submicrometer interconnect performance and systems-on-chip integration," *Proc. IEEE*, vol. 89, no. 5, pp. 602–633, May 2001.

[2] G. L. Loi, B. Agrawal, N. Srivastava, S.-C. Lin, T. Sherwood, and K. Banerjee, "A thermally-aware performance analysis of vertically integrated (3-D) processor-memory hierarchy," in *Proc. 43th ACM/IEEE Des. Automation Conf. (DAC)*, 2006, pp. 991–996.

[3] N. Sillon, A. Astier, H. Boutry, L. Di Cioccio, D. Henry, and P. Leduc, "Enabling technologies for 3D integration: From packaging miniaturization to advanced stacked ICs," in *IEDM Tech. Dig.*, 2008, pp. 595–598.

[4] F. Liu, R. R. Yu, A. M. Young, J. P. Doyle, X. Wang, L. Shi, K.-N. Chen, X. Li, D. A. Dipaola, D. Brown, C. T. Ryan, J. A. Hagan, K. H. Wong, M. Lu, X. Gu, N. R. Klymko, E. D. Perfecto, A. G. Merryman, K. A. Kelly, S. Purushothaman, S. J. Koester, R. Wisnieff, and W. Haensch, "A 300-mm wafer-level three-dimensional integration scheme using tungsten through-silicon via and hybrid Cu-adhesive bonding," in *IEDM Tech. Dig.*, 2008, pp. 599–602.

[5] G. Katti, A. Mercha, J. Van Olmen, C. Huyghebaert, A. Jourdain, M. Stucchi, M. Rakowski, I. Debusschere, P. Soussan, W. Dehaene, K. De Meyer, Y. Travaly, E. Beyne, S. Biesemans, and B. Swinnen, "3D stacked ICs using Cu TSVs and die to wafer hybrid collective bonding," in *IEDM Tech. Dig.*, 2009, pp. 357–360.

[6] L. Cadix, M. Rousseau, C. Fuchs, P. Leduc, A. Thuaire, R. El Farhane, H. Chaabouni, R. Anciant, J.-L. Huguenin, P. Coudrain, A. Farcy, C. Bermond, N. Sillon, B. Fléchet, and P. Ancey, "Integration and frequency dependent electrical modeling of through silicon vias (TSV) for high density 3DICs," in *Int. Interconnect Tech. Conf.*, 2010, pp. 1–3.

[7] G. Katti, M. Stucchi, K. De Meyer, and W. Dehaene, "Electrical modeling and characterization of through silicon via for three-dimensional ICs," *IEEE Trans. Electron Devices*, vol. 57, no. 1, pp. 256–262, Jan. 2010.

[8] Y. Liang and Y. Li, "Closed-form expressions for the resistance and the inductance of different profiles of through-silicon vias," *IEEE Electron Device Lett.*, vol. 32, no. 3, pp. 393–395, Mar. 2011.

[9] I. Savidis and E. G. Friedman, "Closed-form expressions of 3-D via resistance, inductance, and capacitance," *IEEE Trans. Electron Devices*, vol. 56, no. 9, pp. 1873–1881, Sep. 2009.

[10] J. S. Pak, C. Ryu, and J. Kim, "Electrical characterization of through silicon via (TSV) depending on structural and material parameters based on 3D full wave simulation," in *Proc. Int. Conf. Electron. Mater. Packag.*, 2007, pp. 1–6.

[11] C. Xu, H. Li, R. Suaya, and K. Banerjee, "Compact AC modeling and analysis of Cu, W, and CNT based through-silicon vias (TSVs) in 3-D ICs," in *IEDM Tech. Dig.*, 2009, pp. 521–524.

[12] C. Xu, H. Li, R. Suaya, and K. Banerjee, "Compact AC modeling and performance analysis of through-silicon vias in 3-D ICs," *IEEE Trans. Electron Devices*, vol. 57, no. 12, pp. 3405–3417, Dec. 2010.

[13] W. C. Chew, J.-M. Jin, E. Michielssen, and J. Song, *Fast and Efficient Algorithms in Computational Electromagnetics*. Norwood, MA: Artech House, 2001, pp. 730–737.

[14] N. Srivastava, R. Suaya, and K. Banerjee, "Analytical expressions for high-frequency VLSI interconnect impedance extraction in the presence of a multilayer conductive substrate," *IEEE Trans. Comput.-Aided Design Integr. Circuits Syst.*, vol. 28, no. 7, pp. 1047–1060, Jul. 2009.

[15] N. Srivastava, C. Xu, R. Suaya, and K. Banerjee, "Corrections to 'analytical expressions for high-frequency VLSI interconnect impedance extraction in the presence of a multilayer conductive substrate'," *IEEE Trans. Comput.-Aided Design Integr. Circuits Syst.*, vol. 29, no. 5, p. 849, May 2010.

[16] N. Srivastava, R. Suaya, and K. Banerjee, "Efficient 3D high-frequency impedance extraction for general interconnects and inductors above a layered substrate," in *Proc. Des. Test Eur.*, 2010, pp. 459–464.

[17] J. J. Yang, D. G. Fang, and Y. L. Chow, "Discrete complex images of a three-dimensional dipole above and within a lossy ground," *IEE Proc. H*, vol. 138, no. 4, pp. 319–326, Aug. 1991.

[18] T. Moselhy, X. Hu, and L. Daniel, "pFFT in FastMaxwell: A fast impedance extraction solver for 3D conductor structures over substrate," in *Proc. Des., Autom. Test Eur.*, 2007, pp. 1–6.

[19] K. J. Han, M. Swaminathan, and T. Bandyopadhyay, "Electromagnetic modeling of through-silicon via (TSV) interconnections using cylindrical modal basis functions," *IEEE Trans. Adv. Packag.*, vol. 33, no. 4, pp. 804–817, Nov. 2010.

[20] *User's Guide: High Frequency Structure Simulator (HFSSv10.0)*, Ansoft Corporation, Pittsburgh, PA, 2005.

[21] K. A. Michalski and J. R. Mosig, "Multilayered media Green's functions in integral equation formulations," *IEEE Trans. Antennas Propag.*, vol. 45, no. 3, pp. 508–519, Mar. 1997.

[22] K. A. Michalski and D. Zheng, "Electromagnetic scattering and radiation by surfaces of arbitrary shape in layered media, Part I: Theory," *IEEE Trans. Antennas Propag.*, vol. 38, no. 3, pp. 335–344, Mar. 1990.

[23] Maxwell Student Version. [Online]. Available: www.ansoft.com/academic/

Chuan Xu (S'08) received the B.S. degree in microelectronics and the M.S. degree in microelectronics and solid-state electronics from Peking University, Beijing, China, in 2004 and 2007, respectively. During his master's degree, he worked on the fabrication and characterization of AlGaN/GaN heterostructure field-effect transistors. In fall of 2007, he joined the Nanoelectronics Research Laboratory, University of California at Santa Barbara, where he is currently working toward the Ph.D. degree in the Department of Electrical and Computer Engineering.

During the summer of 2008, he was an Intern with the Electrical Interconnect and Packaging (EIP) Group, IBM T. J. Watson Research Center, Yorktown Heights, NY. During the summers of 2009, 2010, and 2011, he was an Intern with the Calibre Division, Mentor Graphics Corporation, Saint Ismier, France. His current research is focused on the modeling, design, and characterization of emerging interconnect materials, structures, and effects.

Mr. Xu was the recipient of the "2008 IBM Problem Solving Award Based on the Use of the EIP Tool Suite," which recognizes outstanding contributions by students in solving the most interesting problems using IBM's Electromagnetic Field Solver Suite of Tools called the EIP tools.

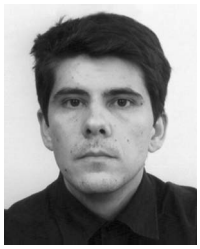

Vassilis Kourkoulos (M'09) received the Diploma from the National Technical University of Athens, Athens, Greece, in 2001 and the M.S. and Ph.D. degrees from the University of Illinois at Urbana-Champaign, in 2004 and 2008, respectively, all in electrical and computer engineering.

Since 2009, he has been with the Calibre Division, Mentor Graphics Corporation, Saint Ismier, France. His research is focused on numerical methods and their applications to computational electromagnetics, advanced interconnects, and 3-D integrated circuits.

Roberto Suaya (M'99–SM'08) received the Ph.D. degree in physics from the University of Buenos Aires, Buenos Aires, Argentina, with his thesis research done at the Stanford Linear Accelerator Center, Stanford University, Stanford, CA.

He held academic positions in theoretical physics with the University of Illinois, Urbana-Champaign, with McGill University, Montreal, QC, Canada, and with Stanford Linear Accelerator Center, and in computer science with California Institute of Technology, Pasadena. He held research positions with Fairchild Research Center, with Schlumberger Palo Alto Research in System Science, with the Computer Science Laboratory, SRI International (formerly Stanford Research Institute), with Weidlinger Associates, and with the Electronics and Information Technology Laboratory (LETI) Research Center of the French Atomic Energy Commission. He is currently the Chief Scientist of the Calibre Division, Mentor Graphics Corporation, Saint Ismier, France. He has been an Entrepreneur in CAD, creating Thunder Software. He has extensively published papers in VLSI CAD and theoretical physics, co-edited a book titled *VLSI and Parallel Computation* (Morgan Kauffman), and extensively lectured in Europe, North and South America, and Asia.

Dr. Suaya is an Associate Editor of the IEEE TRANSACTIONS ON CAD and a member of the Technical Advisory Board of Semiconductor Research Corporation. He has co-chaired international conferences on frontiers in VLSI.

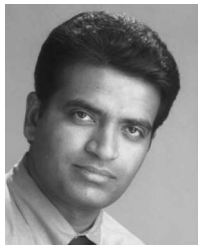

Kaustav Banerjee (S'92–M'99–SM'03) received the Ph.D. degree in electrical engineering and computer sciences from the University of California, Berkeley, in 1999.

In July 2002, he joined the faculty of the Department of Electrical and Computer Engineering, University of California, Santa Barbara (UCSB), where he has been a Full Professor since 2007. At UCSB, he directs the Nanoelectronics Research Laboratory and is an affiliated Faculty with the California NanoSystems Institute and the Institute for Energy Efficiency. Prior to joining UCSB, he was a Research Associate with the Center for Integrated Systems, Stanford University, Stanford, CA from 1999 to 2001. He has also held a number of summer/visiting positions at Texas Instruments, Dallas, from 1993 to 1997; École Polytechnique Fédérale de Lausanne, Switzerland, in 2001; and the Circuits Research Laboratories, Intel Corporation, Hillsboro, OR, in 2002. In December 2010, he held a Visiting Professorship with the Tokyo Institute of Technology, Tokyo, Japan. His research interests include nanometer-scale issues in VLSI as well as circuits and systems issues in emerging nanoelectronics. He is currently involved in exploring the physics, technology, and applications of carbon nanomaterials for next-generation electronics as well as energy harvesting and storage. His research is chronicled in over 220 journal articles, international conference papers, and book chapters, including over 50 invited papers. He is also a Co-editor of the book *Emerging Nanoelectronics: Life With and After CMOS* (Springer-Verlag, 2004).

Prof. Banerjee's technical ideas and innovations have seen widespread proliferation both in the industry and academia as exemplified by his *h-index* of 36 as of April 2011. He has made a number of seminal contributions in the area of nanoscale IC interconnects and innovative interconnect solutions, including 3-D ICs and carbon-based interconnects, which have helped shape the semiconductor industry's R&D efforts in those areas. He has delivered over 100 keynote/panel speeches, tutorials, and invited talks at major international forums and academic/research institutes around the world. His research has also been recognized with numerous awards, including the Best Paper Award at the Design Automation Conference in 2001, the Association of Computing Machinery (ACM) Special Interest Group on Design Automation Outstanding New Faculty Award in 2004, the IEEE Micro Top Picks Award in 2006, and an IBM Faculty Award in 2008. He has served on the Technical and Organizational Committees of several leading IEEE and ACM conferences, including International Electron Devices Meeting, International Reliability Physics Symposium, Design Automation Conference, International Conference on Computer-Aided Design, International Symposium on Quality Electronic Design, and International Conference on Simulation of Semiconductor Processes and Devices. From 2005 to 2008, he served as a member of the Nanotechnology Committee of the IEEE Electron Devices Society (EDS). At present, he serves on the IEEE/EDS VLSI Technology and Circuits Committee. He has been a Distinguished Lecturer of the IEEE Electron Devices Society since 2008.